Exceptionally large room-temperature ferroelectric polarization in the $PbNiO_3$ multiferroic nickelate: First-principles study

X. F. Hao,[1] A. Stroppa,[2] S. Picozzi,[2] A. Filippetti,[3] and C. Franchini[1,*]

[1]*Faculty of Physics, Center for Computational Materials Science, University of Vienna, Wien A-1090, Austria*

[2]*CNR-SPIN L'Aquila, Via Vetoio 10, L'Aquila I-67100, Italy*

[3]*Dipartimento di Fisica, CNR-IOM, UOS Cagliari, Università di Cagliari, Monserrato (CA), Italy*

(Received 6 June 2012; published 30 July 2012)

We present a study based on several advanced first-principles methods of the recently synthesized $PbNiO_3$ [J. Am. Chem. Soc. **133**, 16920 (2011)], a rhombohedral antiferromagnetic insulator, which crystallizes in the highly distorted $R3c$ crystal structure. We find this compound electrically polarized with a very large electric polarization of $\sim$100 $\mu C/cm^2$, thus, even exceeding the polarization of well-known $BiFeO_3$. $PbNiO_3$ is a proper ferroelectric with polarization driven by large Pb-O polar displacements along the [111] direction. Contrary to naive expectations, a definite ionic charge of 4+ for the Pb ion cannot be assigned, and, in fact, the large Pb $6s$-O $2p$ hybridization drives the ferroelectric distortion through a lone-pair mechanism similar to that of other Pb- and Bi-based multiferroics.

DOI: 10.1103/PhysRevB.86.014116 PACS number(s): 77.80.−e, 71.20.−b, 77.22.Ej, 77.84.−s

I. INTRODUCTION

Multiferroics are materials in which different ferroic orders, such as ferromagnetism, ferroelectricity (FE), and/or ferroelasticity may coexist in one single phase.[1] In the past few years, there has been a tremendous boom of interest in these materials due to the potential applications in memory devices or in novel types of magnetic switching in magnetoelectric multiferroics based on the cross coupling between ferroelectric and magnetic channels.[2–4] Furthermore, these materials offer a rich and fascinating playground for the complex physical mechanisms underlying the processes involved in the observed properties.[5] It is obvious that the search and the prediction by material design of new multiferroics is of great importance for both fundamental physics and technological applications.[6,7]

Relatively few multiferroics have been identified so far.[8] Without a doubt, the most studied and well-characterized multiferroic is $BiFeO_3$.[9] It crystallizes in the polar space group $R3c$ (No. 161, point group C_{3v}) and is predicted to have a G-type antiferromagnetic (AFM) alignment of the Fe spins.[6] The $R3c$ symmetry corresponds to the so-called $LiNbO_3$-type structure, which can be viewed as a highly distorted double perovskite with rhombohedral symmetry (see Refs. 10 and 11). The primitive unit cell contains two formula units (ten atoms), arising from counter-rotations of neighboring O octahedra about the [111] axis (see Fig. 1). The crystal symmetry allows the presence of a spontaneous polarization along the [111] direction, which arises from the relative displacement of the Bi sublattices with respect to the FeO_6 octahedra cages along [111]. The origin of the large spontaneous polarization of $Bi^{+3}Fe^{+3}O^{-2}{}_3$, $\sim$90 $\mu C/cm^2$,[9] has been explained by first-principles calculations within the density functional theory plus Hubbard-U approach[12] (DFT + U) and the "modern theory of polarization" (MTP),[13,14] in terms of the lone-pair electrons present at the Bi sites, which are ultimately responsible for the large displacement along the [111] direction.[6]

Inspired by the recent reports of Inaguma *et al.* on the synthesis of a new antiferromagnetically ordered compound with a $LiNbO_3$-type structure, such as $PbNiO_3$,[15,16] here, we explore the possibility of multiferroic behavior in $PbNiO_3$. We first summarize the experimental findings. Inaguma and coworkers synthesized two high-pressure polymorphs of $PbNiO_3$ with (A) a perovskite-type structure and (B) the $LiNbO_3$-type structure;[15,16] the latter (hereafter, called L-$PbNiO_3$) is thermodynamically more stable than the perovskite-type one at ambient pressure. With respect to the orthorhombic structure, in the acentric rhombohedral $LiNbO_3$-type ($R3c$) structure (Fig. 1), Pb and O atoms are displaced against each other along the threefold [111] axis leading to a large distortion of the PbO_6 and NiO_6 octahedra (see Fig. 1). The Pb atom is coordinated by six oxygens at 2.10 and 2.25 Å, whereas, the Ni-O bond distance splits into two subgroups (2.07 and 2.11 Å). Magnetic susceptibility and resistivity measurements indicate that L-$PbNiO_3$ undergoes an AFM transition at $T_N = 205$ K and exhibits semiconducting behavior. The AFM ordering in the acentric crystal structure suggests possible multiferroic behavior.

In the following, we show that L-$PbNiO_3$ is a *new* room-temperature *multiferroic* with an *exceptionally large* polarization (**P**) of about 100 $\mu C/cm^2$, which is the highest polarization ever predicted for any bulk material so far and $\approx$10% larger than that of $BiFeO_3$.[9]

II. COMPUTATIONAL DETAILS

We performed DFT-based calculations using the Vienna *ab initio* simulation package[18] (VASP) based on the projector-augmented-wave method[19,20] within the Perdew, Burke, and Ernzerhof (PBE) parametrization scheme[21] for the generalized gradient approximation (GGA). To overcome the deficiencies of standard exchange-correlation approximations for localized Ni d states, we made use of three beyond-DFT approaches: (i) Dudarev's GGA + U,[12,22] using $U = 4.6$ eV in accordance with the constrained DFT calculation of Ref. 23; (ii) the renowned Heyd-Scuseria-Ernzerhof (HSE) screened hybrid functional,[24] which has been shown to give an excellent account of materials properties for magnetic multiferroics.[25]

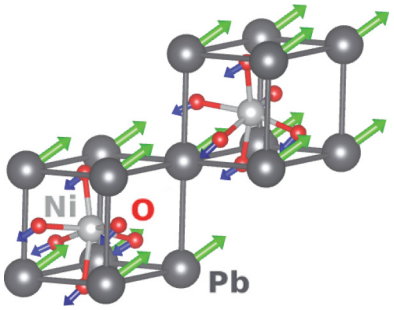

FIG. 1. (Color online) Schematic of the $LiNbO_3$-type $PbNiO_3$ within the space group $R3c$ structure built up from two cubic perovskite unit cells, the black (large), gray (medium), and red (small) spheres denote Pb, Ni, and O atoms, respectively. With respect to the centrosymmetric ($R\bar{3}c$) paraelectric phase (see text), the cations are displaced along the [111] axis relative to the anions (the arrows represent the displacement vectors), and the oxygen octahedra slightly rotate with alternating sense around the [111] direction.[15] The crystal structure was drawn using the program VESTA.[17]

(iii) The recently introduced variational pseudo-self-interaction-correction method[26] (VPSIC) (adopting the HSE optimized structure), implemented within the plane-wave basis set and ultrasoft pseudopotential scheme in the PWSIC code. Although conceptually and technically quite distinct from HSE or GGA + U approaches, the VPSIC compares well with HSE in the description of prototypical strong-correlated oxides MnO and NiO.[27]

The cutoff energy was set as 600 eV, and an $8 \times 8 \times 8$ Monkhorst-Pack grid of k points was used. In HSE, the fraction (1/4) of Fock exchange was sampled using the twofold reduced **k**-point grid to reduce the computational load. The lattice parameters and atomic positions were relaxed (at the GGA + U and HSE levels) until the total energy changed by less than 10^{-5} eV per unit cell and the residual force was smaller than 0.01 eV/Å.

III. RESULTS

In this section, we first present and discuss the ground-state structural, magnetic, and electronic properties of L-$PbNiO_3$, then we report on the ferroelectric properties by evaluating the spontaneous macroscopic polarization **P**.[6]

A. Magnetic, structural, and electronic properties

The G-type antiferromagnetic configuration (AFM-G) in which each Ni ion is surrounded by six nearest-neighbor Ni atoms with opposite spin direction is the most favorable spin configuration with respect to ferromagnetic (by 50 meV/f.u.) [(f.u.) represents formula unit], AFM type-A (by 33 meV/f.u.) and AFM type-C (by 17 meV/f.u.) orderings.

The resulting calculated magnetic Ni magnetic moment (m_{Ni}) is about 1.7μ_B at both GGA + U and HSE levels. The optimized GGA, GGA + U, and HSE structural parameters for the AFM-G phase are listed in Table I. As expected, GGA does not reproduce the experimental values well, whereas, HSE and, to a lesser extent, GGA + U deliver numbers in good agreement with the experiment with relative errors of 1.5%–2% (GGA + U) and <1.0% (HSE).

TABLE I. Structural parameters, magnetic moment, and electronic band gap for the AFM-G configuration of L-$PbNiO_3$ within the GGA, GGA + U, and HSE methods, compared with the available experimental data. a,c are the lattice parameters in the hexagonal setting, whereas, x, y, and z are the internal atomic positions of Pb and O. Ni ions sit in the (6a) (0,0,0) positions. Bond lengths of Pb-O and Ni-O are also reported. Ni-$\widehat{O}$-Ni (°) is the Ni-O-Ni angle. m indicates the magnetic moment of Ni.

	GGA	GGA + U	HSE	Expt.
a (Å)	5.442	5.430	5.359	5.363
c (Å)	13.737	14.353	14.209	14.090
z_{Pb}	0.2226	0.2885	0.2898	0.2864
x_O	0.0605	0.0532	0.0468	0.0487
y_O	0.2598	0.3543	0.3579	0.3657
z_O	0.0931	0.0702	0.0687	0.0668
Ni-O (Å)	2.051	2.128	2.119	2.109
	1.905	2.060	2.053	2.071
Pb-O (Å)	2.395	2.310	2.258	2.246
	2.238	2.174	2.121	2.104
Ni-$\widehat{O}$-Ni (°)	147.8	140.6	138.1	136.7
m_{Ni} (μ_B)	0.97	1.67	1.69	
gap (eV)	Metallic	0.37	1.18	

The drawbacks of conventional GGA are more dramatic for the electronic properties. The GGA scheme finds a metallic character in clear disagreement with the experiment.[15] Conversely, the inclusion of either the on-site U or the Fock exchange cures this limitation and correctly predicts an insulating state with an energy gap of ∼0.4 eV (GGA + U) and ∼1.2 eV (HSE) as inferred from the density of states (DOS) shown in Fig. 2. The VPSIC gap is 0.9 eV, satisfactorily similar to the HSE value. The gap opens between occupied Ni d and O p states and the lowest unoccupied electronic states that are made up by a mixture of Pb s and O s states.

Spin polarization does not affect Pb and O DOS, whereas, the Ni atoms display a magnetic moment of 1.69μ_B. In hexagonal coordinates (with z parallel to the [111] direction) the Ni d states are distributed into two doublets (d_{xy},$d_{x^2-y^2}$) and (d_{xz},d_{yz}), which contribute to the net magnetization by 0.65 and 1.65μ_B, respectively, and a spin degenerate d_{z^2} singlet. The broad Ni 3d valence manifold is strongly hybridized with the O 2p states and lies in the energy range between −6 eV and the Fermi level.

The most important feature of the DOS is at the bottom of the valence region, between −9 and −6 eV: a large region dominated by highly hybridized Pb 6s and O 2p states. The presence of a substantial amount of charge (about one electron, see Fig. 3) within the Pb 6s orbital is at odds with the nominal Pb^{4+} valence originally assumed in the interpretation of x-ray photoemission spectroscopy results.[15,16] In realistic calculations, substantial deviation between the static charges and the nominal ionic charges (due to large hybridization effects) is the rule rather than the exception, thus, it certainly does not come as a surprise. In this case, however, this deviation is worthy of being emphasized since, as we show below, it is strictly connected to the ferroelectric instability.

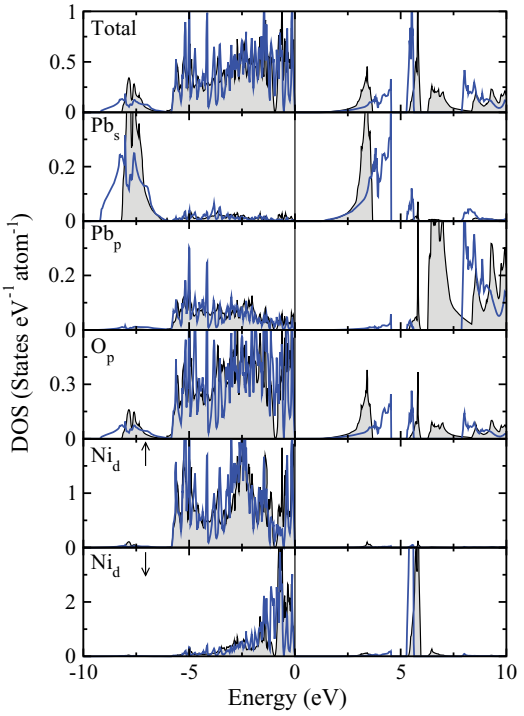

FIG. 2. (Color online) HSE calculated total and site-decomposed density of states for the AFM-G type $PbNiO_3$ in the acentric $R3c$ (full lines) and centric $R\bar{3}c$ (shadow) phases. The vertical lines denote the Fermi level. Up and down arrows indicate spin-up and spin-down components, respectively.

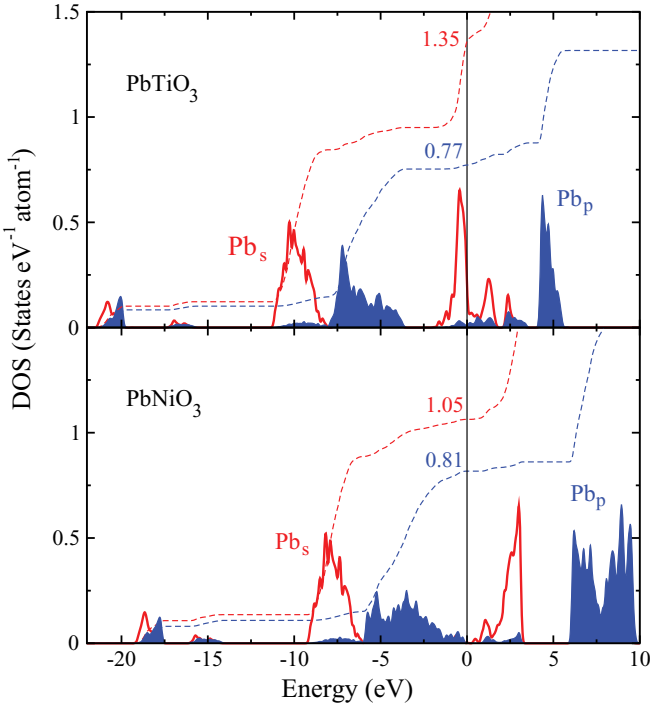

FIG. 3. (Color online) Pb s (light gray, full line) and Pb p (dark gray, shadow) DOS and integrated DOS of Pb in $PbTiO_3$ and ($PbNiO_3$) computed by VASP. The integration was performed using the standard Wigner-Seitz radius employed in the VASP pseudopotential database (Pb: 1.725 Å, Ti: 1.323 Å, Ni: 1.28 Å, O: 0.900 Å).

As the charge density stored in the Pb s orbital is a key ingredient to explain the multiferroic behavior of $PbNiO_3$ in Fig. 3, we describe this aspect in detail by comparing the Pb DOS of $PbNiO_3$ calculated within HSE with the same quantity of $PbNiO_3$ where Pb is assumed to be a 2+ ion. Also, we compare Pb DOS in $PbNiO_3$ and Bi DOS in $BiFeO_3$ (Fig. 4), which is nominally Bi^{3+}.

The presence of a considerable portion of occupied Pb s and (a minor extent) p states in $PbNiO_3$ unambiguously shows that Pb does not donate all its $6s^2p^2$ electrons to end up in a 4+ valence.[28,29] In fact, by DOS integration, we find Pb to accommodate a similar amount of charge in $PbNiO_3$ and $PbTiO_3$: 1.86 electrons in $PbNiO_3$ and 2.21 electrons in $PbTiO_3$, respectively, further distributed in s states (1.05 electrons for $PbNiO_3$ vs 1.35 electrons for $PbTiO_3$) and p states (0.81 electrons for $PbNiO_3$ vs 0.77 electrons for $PbTiO_3$). For what concerns the comparison with the Bi DOS in $BiFeO_3$, we can notice a sensible difference in the s charge (1.63 electrons for Bi against 1.05 electrons for Pb) and a substantial equivalence for what concerns the p charge (about 0.8 electrons for both ions). Notice also, in Fig. 4, that although, Fe and Ni $3d$ charges in $BiFeO_3$ and $PbNiO_3$ are substantially close to their nominal d^5 and d^8 values, the O p charge is much smaller than its nominal p^6 as a consequence of the strong hybridization with the Pb (or Bi) sp charge. In other words, a consistent portion of the nominal (i.e., presumed) O p charge is actually stretched onto the Pb or Bi sp orbitals.

To highlight the role of the Pb $6s$-O $2p$ hybridization, in Fig. 2, we show the DOS for the centrosymmetric nonpolar reference structure $R\bar{3}c$ as well as the polar structure: The major difference is indeed the 2-eV downshift and the broadening (more than a factor-2 bandwidth expansion) of the Pb $6s$-O $2p$ spectral weight occurring along with the centrosymmetric-to-ferroelectric transformation. This so-called stereochemical activity of the A-site cation[30,31] is quite consistent with what occurs in Bi-based [$BiFeO_3$,[6] $BiMnO_3$ (Refs. 30 and 31)] and Pb-based [$PbTiO_3$ (Ref. 32)] compounds, usually labeled as lone-pair ferroelectrics (see Figs. 3 and 4). Thus, although smaller than the Pb charge in $PbTiO_3$ or the Bi charge in $BiFeO_3$ ($1.63e^-$) (see Figs. 3 and 4), the Pb charge in $PbNiO_3$ is far from vanishing and, in fact, is large enough to justify the active role of Pb in the stabilization of ferroelectric distortions. This is also reflected in the structural distortions, which *predominantly* involve counterdisplacements of Pb and O atoms along the [111] direction (see Fig. 1). Our analysis gives clear evidence that the heuristic concept of nominal valence charge, while useful to qualitatively describe the chemical characteristics of a system, is insufficient for the correct interpretation of such a sophisticated mechanism as the ferroelectric distortion, which is crucially affected by the detailed competition between hybridization and charge-transfer effects and then requires the accurate quantitative evaluation of structural and electronic properties.

B. Analysis of ferroelectric polarization

By pseudosymmetry analysis,[33] we determine a parent centrosymmetric structure ($R\bar{3}c$) with minimal supergroup symmetries from which the observed noncentrosymmetric

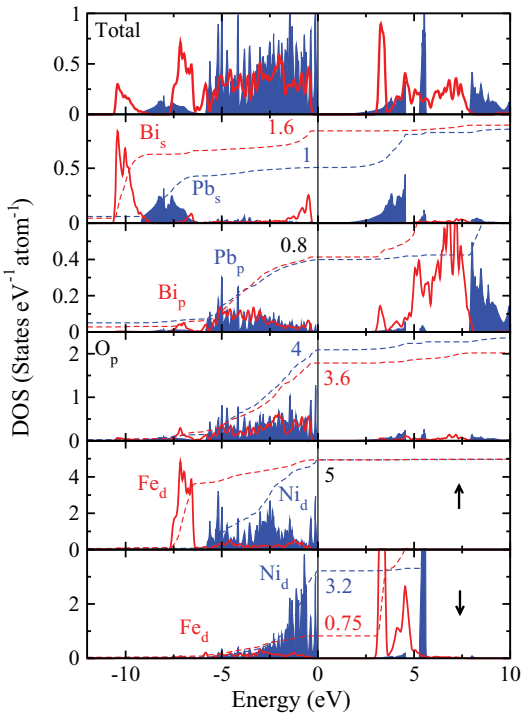

FIG. 4. (Color online) Comparison between the $PbNiO_3$ (dark gray, shadow) and $BiFeO_3$ (light gray, full line) DOS. The numbers refer to the integrated charge for both spin channels. Up and down arrows indicate spin-up and spin-down components, respectively.

structure can be reached through a continuous structural distortion. By definition, the polarization is zero (modulo a polarization quantum[13,14]) in this paraelectric (PE) phase ($\lambda = 0$), thus, it represents a viable reference state for the evaluation of the polarization in the polar structure ($\lambda = 1$). Here, $\lambda = 1$ is the amplitude of the polar distortion, which progressively transforms the $R\bar{3}c$ phase into the $R3c$ one. For consistency, we assume, for the $R\bar{3}c$ phase, the same volume and rhombohedral angle of the polar structure.

In the PE phase, Pb and O atoms lie in (111) PbO_3 planes. Symmetry mode analysis shows that the $\lambda = [0,1]$ transformation (shown by arrows in Fig. 1) is almost exclusively composed by an in-phase [111]-parallel relative shift in Pb and O atoms (i.e., a nearly exclusive Γ_{2-}-mode transformation), with some very residual O-rotation contributions. The Pb atoms are displaced from their positions by 0.56 Å, and the O atoms are displaced from their positions by 0.23 Å, whereas, Ni atoms are almost unchanged. This transformation produces an alternate shrinking and dilatation of Pb-O distances along [111] of about 0.8 Å, whereas Ni (111) planes are left off centered by 0.17 Å with respect to their adjacent PbO_3 planes. The total polarization **P** can be split as the sum of ionic P_{ion} and electronic contribution P_{ele}: The former is the dipole of the ion-core charges; the latter is obtained by the Berry phase approach within the MTP.[13,14] HSE and VPSIC describe both polar and nonpolar structures as insulating, whereas, within GGA + U, a large $U = 7.6$ eV is required to open a gap in the PE phase. The HSE-calculated DOS shown in Fig. 2 indicates that the value of the gap is essentially the same for both acentric $R3c$ and nonpolar $R\bar{3}c$ phases. Figure 5 displays

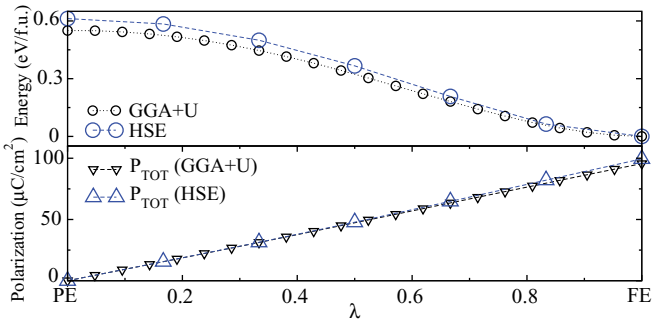

FIG. 5. (Color online) Total energy profile E, total polarization $\mathbf{P}_{tot}$ as a function of the polar distortion λ from the $\lambda = 0$ PE phase to the $\lambda = 1$ FE one. Both HSE (dashed lines, dark) and GGA + U (dotted lines, gray) data are displayed.

total energy and polarization $\mathbf{P}_{tot}$ as a function of the polar distortion λ at both the HSE and the PBE + U levels. Both methods deliver the same outcome. As expected, the polar structure is more stable than the nonpolar one by 0.6 eV/f.u (0.7 eV/f.u. according to VPSIC). Both $\mathbf{P}_{ion}$ and $\mathbf{P}_{ele}$ grow monotonically with the polar distortion, giving rise to a total polarization $\mathbf{P}_{tot}$ of $\sim$100 μC/cm^2 (98.5 μC/cm^2 according to VPSIC), thus, $\approx$10% larger than that of $BiFeO_3$ (Refs. 6 and 25) and significantly enhanced with respect to that of $LiNbO_3$ (80 μC/cm^2)[10] and $ZnSnO_3$ (57 μC/cm^2).[34]

We have also evaluated the polarization using the approximated expression $\mathbf{P}_{tot} = \sum_i \Delta R_i Z_i^*$, where ΔR_i are atomic displacements (from centrosymmetric to polar structures) and Z_i^* are Born effective charges (BECs) calculated via linear-response formalism in GGA + U. We obtain a value (93.8 μC/cm^2) substantially similar to the evaluation based on the exact Berry phase formula. We found a nearly isotropic BEC tensor and dynamical charges similar in both PE and FE phases (see Table II). For Pb, we obtained an anomalous BEC value of 4.4 (as compared to the static charge $\approx$2.15), identical to the Bi BEC calculated in $BiFeO_3$, coherently with the role of this ion in guiding the ferroelectric transition.[9]

C. Summary

Using several beyond-local density approximation (LDA) methods (LDA + U, HSE, and VPSIC) and the MTP approach for the determination of polarization properties, we report the presence of a large spontaneous electric polarization $\sim$100 μC/cm^2 in rhombohedral $PbNiO_3$ associated with the structural transformation from the centrosymmetric $R\bar{3}c$ to the polar $R3c$ symmetry. The microscopic analysis shows that this proper ferroelectric instability is dominated by huge in-phase (i.e., Γ-mode) relative displacements of Pb and on-top O atoms along the [111] direction, in turn, associated with

TABLE II. Born effective charges for Pb and Ni in $PbNiO_3$ (with ferroelectric and paraelectric phases) computed via linear-response formalism within the GGA + U method.

	Pb	Ni	O
$R3c$ (FE)	4.40	1.97	−2.12
$R\bar{3}c$ (PE)	4.41	1.97	−2.12

large Pb *s*-O *p* band rehybridization at the bottom of the valence-band manifold. This ferroelectric mechanism can then be assimilated to other Bi-based and Pb-based ferroelectrics, whereas, the naive interpretation of Pb as an inactive +4-charged ion would be totally misleading. This material may be a prototype of a new class of Ni-based rhombohedral multiferroics, which take advantage of the stable rhombohedral symmetry to develop large ferroelectric displacements along the [111] axis and still maintain strong magnetic coupling in the Ni sublattice.

ACKNOWLEDGMENTS

Support by the European Community (FP7 EU-INDIA grant ATHENA and ERC Starting Grant No. 203523 BISMUTH) is gratefully acknowledged. X.H. thanks C. Ederer and C.-Y. Ren for their helpful advice and comments. A.S. thanks J. M. Perez-Mato for useful discussions. The calculations have been performed on the Vienna Scientific Cluster (VSC) and, partially, in the CASPUR Supercomputing Center in Rome.

*Corresponding author: cesare.franchini@univie.ac.at

[1] D. I. Khomskii, Phys. **2**, 20 (2009).
[2] T. Kimura *et al*., Nature (London) **426**, 55 (2003).
[3] N. Hur, S. Park, P. A. Sharma, J. S. Guha, and S.-W. Cheong, Nature (London) **429**, 392 (2003).
[4] S.-W. Cheong and M. Mostovoy, Nature Mater. **6**, 13 (2007).
[5] I. B. Bersuker, Phys. Rev. Lett. **108**, 137202 (2012).
[6] J. B. Neaton, C. Ederer, U. V. Waghmare, N. A. Spaldin, and K. M. Rabe, Phys. Rev. B **71**, 014113 (2005).
[7] C. J. Fennie, Phys. Rev. Lett. **100**, 167203 (2008).
[8] N. A. Hill, J. Phys. Chem. B **104**, 6694 (2000).
[9] J. Wang *et al*., Science **299**, 1719 (2003).
[10] M. Veithen and P. Ghosez, Phys. Rev. B **65**, 214302 (2002).
[11] A. M. Glass and M. E. Lines, Phys. Rev. B **13**, 180 (1976).
[12] V. I. Anisimov, F. Aryasetiawan, and A. I. Lichtenstein, J. Phys.: Condens. Matter **9**, 767 (1997).
[13] R. D. King-Smith and D. Vanderbilt, Phys. Rev. B **47**, 1651 (1993); D. Vanderbilt and R. D. King-Smith, *ibid*. **48**, 4442 (1993).
[14] R. Resta, Rev. Mod. Phys. **66**, 899 (1994).
[15] Y. Inaguma *et al*., J. Am. Chem. Soc. **133**, 16920 (2011).
[16] Y. Inaguma *et al*., J. Phys.: Conf. Ser. **215**, 012131 (2010).
[17] K. Momma and F. Izumi, J. Appl. Crystallogr. **41**, 653 (2008).
[18] G. Kresse and J. Hafner, Phys. Rev. B **48**, 13115 (1993); G. Kresse and J. Furthmüller, Comput. Mater. Sci. **6**, 15 (1996).
[19] P. E. Blöchl, Phys. Rev. B **50**, 17953 (1994).
[20] G. Kresse and D. Joubert, Phys. Rev. B **59**, 1758 (1999).
[21] J. P. Perdew, K. Burke, and M. Ernzerhof, Phys. Rev. Lett. **77**, 3865 (1996).
[22] S. L. Dudarev, G. A. Botton, S. Y. Savrasov, C. J. Humphreys, and A. P. Sutton, Phys. Rev. B **57**, 1505 (1998).
[23] M. Cococcioni and S. de Gironcoli, Phys. Rev. B **71**, 035105 (2005).
[24] J. Heyd, G. E. Scuseria, and M. Ernzerhof, J. Chem. Phys. **118**, 8207 (2003); **124**, 219906 (2006).
[25] A. Stroppa, and S. Picozzi, Phys. Chem. Chem. Phys. **12**, 5405 (2010).
[26] A. Filippetti, C. D. Pemmaraju, S. Sanvito, P. Delugas, D. Puggioni, and V. Fiorentini, Phys. Rev. B **84**, 195127 (2011).
[27] T. Archer, C. D. Pemmaraju and S. Sanvito, C. Franchini, J. He, A. Filippetti, P. Delugas, D. Puggioni, V. Fiorentini, R. Tiwari, and P. Majumdar, Phys. Rev. B **84**, 115114 (2011).
[28] D. O. Scanlon, A. B. Kehoe, G. W. Watson, M. O. Jones, W. I. F. David, D. J. Payne, R. G. Egdell, P. P. Edwards, and A. Walsh, Phys. Rev. Lett. **107**, 246402 (2011).
[29] G. W. Watson, S. C. Parker, and G. Kresse, Phys. Rev. B **59**, 8481 (1999).
[30] R. Seshadri and N. A. Hill, Chem. Mater. **13**, 2892 (2001).
[31] N. A. Hill and K. M. Rabe, Phys. Rev. B **59**, 8759 (1999).
[32] R. E. Cohen, Nature (London) **358**, 136 (1992).
[33] M. I. Aroyo *et al*., Z. Kristallogr. **221**, 15 (2006); Acta Cryst. A **62**, 115 (2006).
[34] M. Nakayama, M. Nogami, M. Yoshida, T. Katsumata, and Y. Inaguma, Adv. Mater. **22**, 2579 (2010).